ADVANCED FUNCTIONAL MATERIALS



# Electric-Field-Directed Growth of Gold Nanorods in Aqueous Surfactant Solutions**

By *Jorge Pérez-Juste*, *Luis M. Liz-Marzán*, *Steven Carnie*, *Derek Y. C. Chan*, and *Paul Mulvaney**

The factors affecting the nucleation and growth of gold nanorods, (Jana et al., *Adv. Mater.* **2001**, *13*, 1389) have been investigated. It is shown that the size and aspect ratio can be controlled through the use of different sized seed particles. The length of the rods can be tuned from 25–170 nm, while the width remains almost constant at 22–25 nm. The formation of rods requires the presence of the cationic surfactant cetyltrimethylammonium bromide (CTAB). Lower temperature favors rod formation, although this reduces CTAB solubility. The addition of chloride ions or the use of dodecyltrimethylammonium bromide (DTAB) leads to shorter-aspect rods. $Au^{III}$ and $Au^{I}$ are shown to be quantitatively bound to the CTAB micelles. We propose an electrochemical mechanism for rod formation, whereby the flux of $Au^{I}$ bound to cationic micelles to the seed surface is maximized at points of highest curvature, where the electrical double layer gradient is highest. Initial numerical solutions to the electric potential and field around an ellipsoid in a 1:1 electrolyte are provided, which indicate that the field at the particle tip scales linearly with the aspect ratio. Mean free passage times for ions are found to be shortest at the tips. The results provide a general explanation for the formation of non-equilibrium crystal habits and a mechanism for controlling crystal growth.

## 1. Introduction

A key goal in current materials science research is to understand the mechanisms that determine crystal habit and the shape of crystals following homogeneous nucleation in solution. Ultimately, it should become possible to grow crystals of any desired orientation, shape, and crystal structure. Gold provides an interesting case, because the lattice is composed of a single element displaying a simple face-centered cubic (fcc) crystal structure. The surface energies of most facets are quite similar, with the [111] face being the most stable. This facet also has the largest work function, which is important during redox reactions such as those occurring during crystal growth. There are now several reported synthetic methods for producing not only monodisperse gold spheres[1] but also triangular prisms[2,3] and small gold rods directly in solution. Pileni and colleagues have achieved good shape control of copper nanocrystals in microemulsion systems.[4] Originally, gold nanorods had been fabricated using porous alumina films as a template, but the amounts that could be made this way were very small.[5] However, considerable basic work on the optical properties and alignment of these rods could be carried out.[5–7] Wang et al. subsequently reported a novel electrochemical synthesis of gold nanorods in the presence of cationic surfactants, rod inducing co-surfactants, and other additives, that were found empirically to favor rod formation.[8,9] This synthesis represents a landmark in terms of shape control of metal particles. Subsequently, Murphy and coworkers and then Yang et al. discovered reduction conditions that enable the entire synthesis to be carried out directly in solution.[10–12] Their protocols enable excellent aspect ratio control, but both groups of researchers stated that aspect ratio control required the addition of silver ions.[13] A mechanism for rod formation could not be provided. The seed mediated method was further improved by El-Sayed and coworkers,[14] who made two significant modifications to the seed-mediated growth method: a) replacement of the sodium citrate with cetyltrimethylammonium bromide (CTAB) molecules in the seed formation step; and b) adjustment of the silver content of the growth solution to grow nanorods with controlled aspect ratios. This resulted in the formation of < 1 % gold spheres.

In this paper we examine the nucleation and growth conditions more closely, and we pinpoint the parameters that induce the growth of rod-like particles. Binding of the $Au^{III}$ and $Au^{I}$ ions into the cationic micelles present in solution is shown to be the key phenomenon. This means that gold ions can be reduced only as micelles approach the seed particles. This approach is strongly influenced by the local, electrical double-layer interaction. The flux of solution-phase ions and micelles to the gold seed particle surface in the presence of this field will be shown to increase with the local curvature and leads to preferential growth at the tips. The model explains qualitatively the effects of various preparation conditions on the rod yield and aspect ratio. While the mechanism may not apply to all cases of surfactant-mediated growth, it provides a mechanism for steering surfactant-"directed" growth in aqueous solution.

[*] Prof. P. Mulvaney, Dr. J. Pérez-Juste
School of Chemistry, University of Melbourne
Parkville, VIC, 3010 (Australia)
Email: mulvaney@unimelb.edu.au
Prof. L. M. Liz-Marzán
Departamento de Química Física
Universidade de Vigo
Vigo, 36200 (Spain)
Prof. S. Carnie, Prof. D. Y. C. Chan
Dept. Maths and Statistics, University of Melbourne
Parkville, VIC, 3010 (Australia)

[**] Supporting Information is available online from WileyInterscience or from the author.

 DOI: 10.1002/adfm.200305068  

## 2. Results

The results presented here pertain to the optimization of the rod synthesis and the isolation of factors that are important for obtaining rods rather than spheres. Small spherical gold seeds are prepared using a strong nucleating agent ($NaBH_4$). Citrate is added as a stabilizer, yielding negatively charged particles with a zeta potential of about –40 mV.[15] Secondary solutions of $HAuCl_4$ and ascorbic acid, a weak reductant, as well as CTAB, a cationic surfactant, are then mixed with the seed. The ascorbate anion transfers electrons to the seed particles, which then reduce the gold ions to form a gold shell, which grows as a rod. Numerous factors affect the aspect ratio and yield of the gold rods, and these are now addressed in turn.

### 2.1. Influence of the Amount of Seed

Initial results with seed particles prepared using Murphy's route revealed that the age of the seeds is critical for reproducible results. Seed solutions older than several hours behaved differently, and made comparative experiments impractical.[11] The 3.5 nm Au citrate seed solution prepared by the current procedure (see Experimental section) enable the same rods to be produced over a period of up to one month. We believe the more stable seed is due to the use of lower gold concentrations and the decomposition of the excess $NaBH_4$ by gentle heating after preparation, which reduces inadvertent nucleation during rod growth. Figure 1 shows the spectra of gold nanorods prepared using different concentrations of 3.5 nm Au citrate seed concentrations. As the concentration of seed particles is decreased, the aspect ratio increases.

The better seed synthesis improves the yield of rods considerably. More importantly, in stark contrast to the earlier researchers, we found that it was possible to alter the aspect ratio without adding any further additives such as silver nitrate.[9,11] Initially, Murphy and coworkers reported that the presence of $AgNO_3$ was essential for producing and controlling "the aspect ratio of the spheroids and the aspect ratio (at least for low aspect ratio, between 1 and 6) could not be controlled by varying the seed-to-metal-salt ratio when silver ions were not present".[11] Yang's photochemical method and El-Sayed's protocols also required silver ions.[12,14] However, we note from the experiments at 20 °C that the gold nanorods have a rod-like instead of a needle-like morphology, as found in the presence of $AgNO_3$.

Figure 2 shows the visible spectra at different stages of the rod growth. Under these experimental conditions the seed-mediated growth kinetics are clearly slower than those in the absence of CTAB, where growth takes place within the first few seconds after mixing.[16] It is difficult to see at first sight why the CTAB can retard the rate of reduction of gold by a factor of 100–1000.

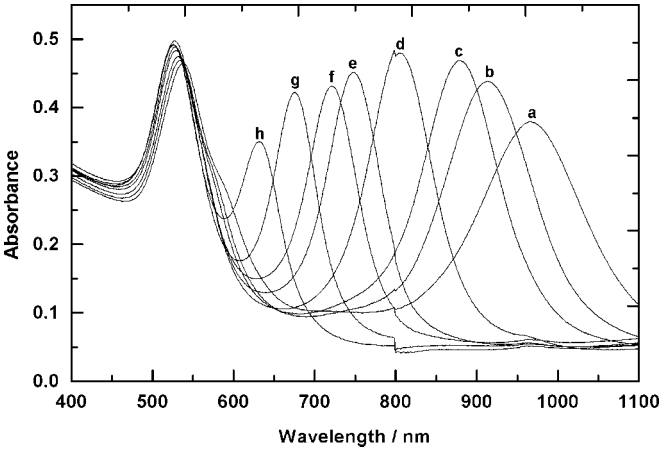


**Figure 1.** Spectra of Au nanorods with increasing aspect ratios formed by decreasing the amount of Au-citrate seed; a) 0.010 mL, b) 0.015 mL, c) 0.020 mL, d) 0.030 mL, e) 0.040 mL, f) 0.050 mL, g) 0.07 mL, h) 0.10 mL. [Au] = $1.25 \times 10^{-4}$ M, [CTAB] = 0.008 M, and $T$ = 20 °C in all cases.

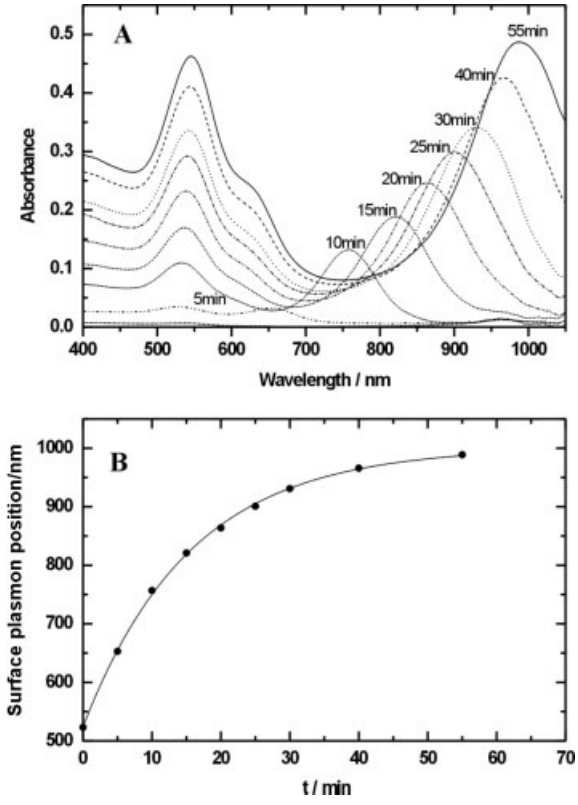


**Figure 2.** A) UV-vis spectra showing the growth of a gold nanorod solution after addition of 0.01 mL of a seed solution pre-coated with CTAB. [Au] = 0.125 mM, [CTAB] = 8.0 mM and $T$ = 20 °C. B) Variation of the longitudinal surface plasmon band position with time during growth. Conditions as per Figure 2A.

### 2.2. Inversion versus Agitation

A second factor that appears to be important is the method of mixing seed and growth solutions. Rod synthesis was reported to work only if the solutions are briefly mixed and allowed to grow in a quiescent solution.[12] We also observed that the aspect ratio and yield of rods depended on the mixing protocols.[10,17] This was re-investigated using the improved seed syn-

  

ADVANCED FUNCTIONAL MATERIALS



thesis. Figure S2 in the Supporting Information shows the spectra of the Au nanorods synthesized in stirred reaction vessels and it can be safely concluded that, under optimal conditions, stirring does not adversely affect rod formation. This immediately implies that rods still form in solutions where there is a homogeneous distribution of reactants, and that there is a surface mechanism for ensuring reduction takes place preferentially at the particle tips.

### 2.3. Coagulation of the Seed

A further potential experimental difficulty is the addition of the citrate/borate stabilized seed solutions to the cationic surfactants prior to gold rod formation. We find the reversal of zeta potential associated with this process can lead to aggregates, which may themselves provide nuclei for rod formation. One might hypothesize that dimers or trimers formed during charge reversal may act as the seeds for rod formation. We therefore compared naked seed solutions with CTAB capped seeds. 0.3 mL of citrate stabilized Au was added dropwise while stirring to 0.3 mL 0.01 M CTAB (i.e., $[Au] = 6.25 \times 10^{-5}$ M and [CTAB] = 0.005 M final concentrations) to create cationic gold seeds. There were no changes in the absorption spectra of the gold colloids, and no significant aggregation took place during this process, as determined by transmission electron microscopy (TEM). The experiments in Figure 1 were repeated with these CTAB coated gold seeds. Figure 3 shows the spectra of the nanorods obtained. From a comparison with Figure 1, it is clear that the yield in the case of CTAB capped seeds is much higher, as evident from the higher intensity of the SPL (longitudinal surface plasmon) band compared to the SPT (transverse surface plasmon) absorption band. This indicates that the more colloidally stable the Au seed particles are, the better the yield of rods.

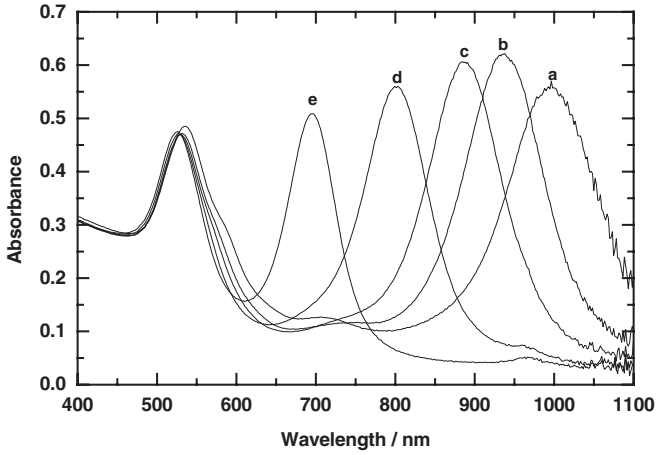


**Figure 3.** Effect of the seed particle concentration on the spectra of Au nanorods. The seed was pre-coated with CTAB (see text for details). Volume of seed solutions are: a) 0.010 mL, b) 0.015 mL, c) 0.020 mL, d) 0.030 mL, e) 0.050 mL. $[Au] = 1.25 \times 10^{-4}$ M, [CTAB] = 0.008 M, and $T = 20$ °C in all cases.

### 2.4. Influence of the Seed Size and Preparation Route

In accord with the experience of the Murphy group, the seed solution is critical for rod formation. Experiments carried out with other types of gold seeds almost invariably led to spherical particles or low yields of rods. We prepared 2 nm gold seeds using carbon disulfide[18] and tetrakis(hydroxymethyl)phosphonium chloride (THPC)[19] as reductants. Neither of these seeds yielded rods during growth. To establish whether the seed size is critical, and whether the aspect ratio and rod width can be influenced by the use of different seed sizes, we prepared 3.5 nm Au seeds and then used these to grow 5.5 nm and 7.0 nm Au seed particles using the seeded-growth method published by Murphy.[20] Spectra of the resultant seed solutions are provided in the Supporting Information. Figures 4A,B show the influence of seed concentration on the aspect ratio of the gold rods. We obtained reproducible and tunable nanorod preparation from Au–CTAB nanoparticles of different lengths. Note that the Au concentration in the seed solutions is the same ($[Au] = 1.25 \times 10^{-4}$ M) in each experiment, but the number of rods decreases because of the increasing seed size. To keep the number of seed nuclei added comparable (and therefore, the

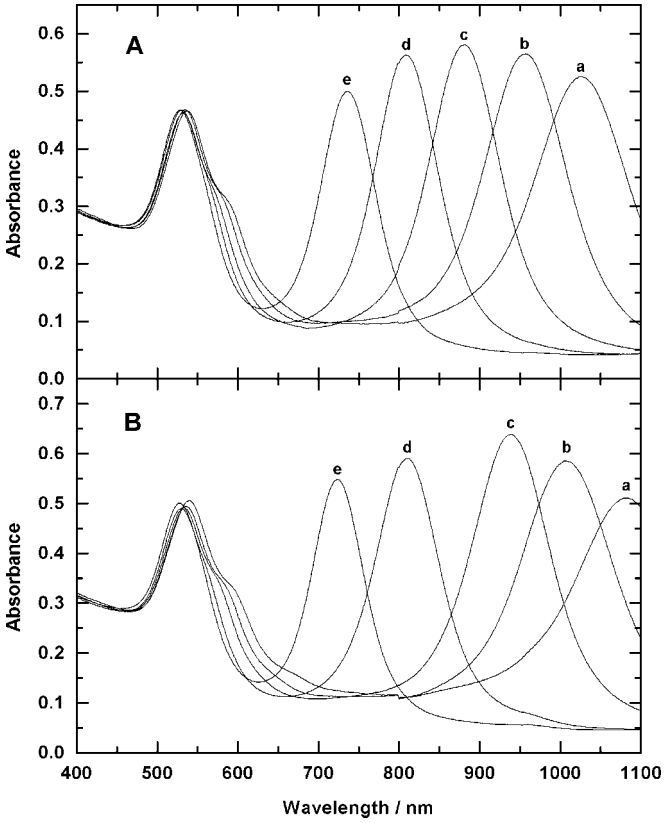


**Figure 4.** A) Spectra of Au nanorods with increasing aspect ratios formed by decreasing the amount of 5.5 nm CTAB-coated Au seed particles added. a) 0.051 mL, b) 0.068 mL, c) 0.102 mL, d) 0.175 mL, e) 0.262 mL. B) Spectra of Au nanorods with increasing aspect ratios formed by decreasing the amount of 7.0 nm CTAB-coated Au seed particles added. a) 0.15 mL, b) 0.20 mL, c) 0.30 mL, d) 0.40 mL, e) 0.60 mL. $[AuCl_4^-] = 1.25 \times 10^{-4}$ M, [CTAB] = 0.008 M, and $T = 20$ °C in all cases.

  

number and the size of the rods) it is necessary to increase the volume of seed added as the seed size is increased. Figure 5 shows TEM images of samples obtained from both 5.5 nm and 7.0 nm seeds. Surprisingly, although the aspect ratio can be systematically varied through the seed concentration, the width of the gold rods remains almost constant for 3.5, 5.5, and 7.0 nm Au–CTAB seed particles.

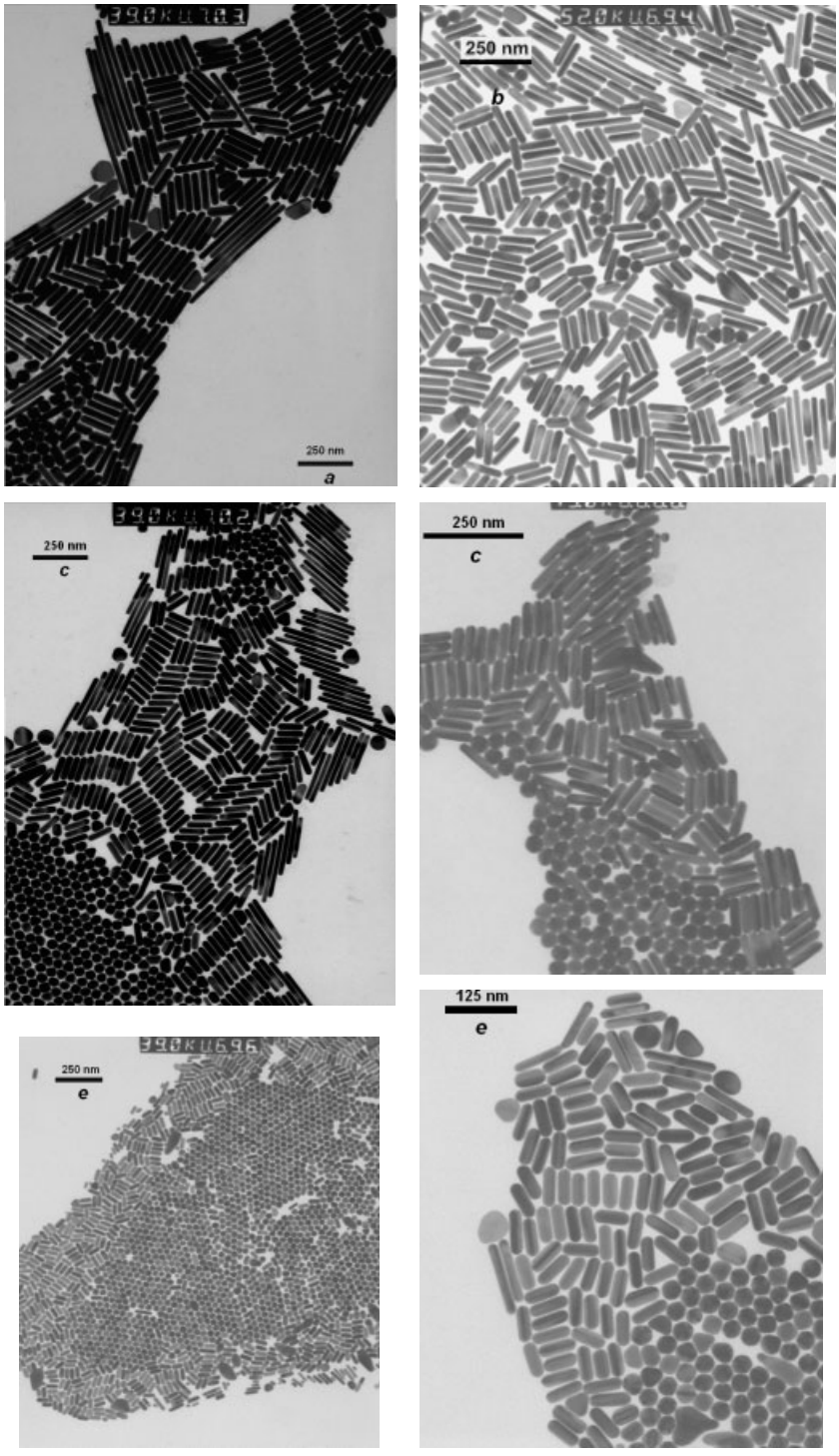


**Figure 5.** (Left): TEM images of the *b*, *c*, and *e* samples of Figure 4A obtained from the 5.5 nm seeds. (Right): TEM images of the *a*, *c*, and *e* samples in Figure 4B obtained from 7.0 nm seeds.

### 2.5. Influence of a Cosurfactant

Clearly, the most important factor leading to rod formation is the presence of the cationic surfactant. To understand why CTAB influences the particle morphology, we now try to analyze the effects of the surfactant counterions and the hydrophobic carbon tail separately. Different experiments have been performed keeping the CTAB concentration (0.008 M) and the amount of seed added (0.01 mL) constant, while varying the amount of an added cosurfactant. We compared the rod forming ability of cetyltrimethylammonium chloride (CTAC), a surfactant with the same number of carbon atoms but with chloride as the counterion, and decyltrimethylammonium bromide (DTAB), a surfactant with the same counterion but with just twelve carbon atoms in the hydrophobic chain. Figure 6A shows how an increase in the added CTAC concentration decreases the aspect ratio of the nanorods formed, as well as the percentage of nanorods formed. Figure 6B shows the absorption spectra of the nanorods synthesized in the presence of different NaCl concentrations. Chloride ions have a similar effect on the aspect ratio as does CTAC, due to the exchange of chloride and bromide counterions around the CTAB micelles in solution ($K_{Br}^{Cl} = 0.3$).[21] Changing the counterion is known to have a strong effect on the solution behavior of quaternary ammonium surfactants. Critical micelle concentration (cmc), micelle shape, and phase equilibria are all influenced by the effect of counterion binding.[22,23] All experimental studies agree on the binding order: $Cl^- < Br^-$ to the surfactant head group.[24] The addition of NaCl produces a decrease in the cmc and the aggregation number of the micellar systems, while conversely, the addition of CTAC increases the cmc and the micelle aggregation number. Nevertheless, addition of either reagent results in a poorer yield of gold rods.

A similar trend is observed for rod growth in the presence of increasing concentrations of DTAB, as shown in Figure 7. However, the concentration of cosurfactant necessary to completely suppress nanorod formation is higher (3 mM for CTAC and 10 mM for DTAB). DTAB primarily reduces the yield of rods, while the CTAC primarily affects the ratio of rods to spheres formed during growth. The DTAB effect can be ascribed to a change in the CTAB micellar system; the critical micelle concentration of the CTAB/DTAB mixed systems will increase as DTAB is

  

ADVANCED FUNCTIONAL MATERIALS



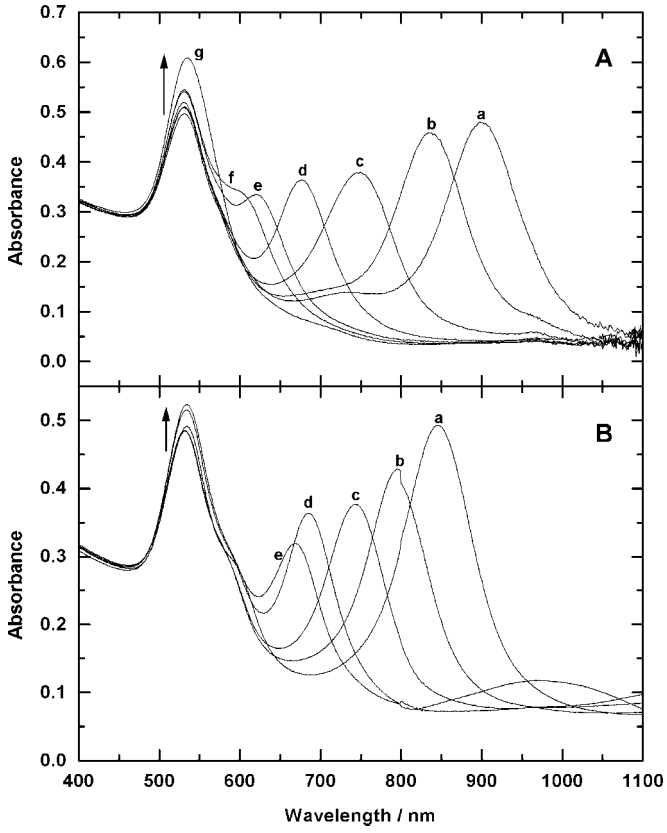


**Figure 6.** A) Influence of the CTAC concentration on the aspect ratio and yield of the Au nanorods; a) 0, b) 0.5 mM, c) 1 mM, d) 2 mM, e) 2.5 mM, f) 3 mM, g) 4 mM CTAC. B) Influence of the NaCl concentration on the aspect ratio and yield of the Au nanorods; a) 0, b) 0.5 mM, c) 1 mM, d) 2 mM, e) 3 mM NaCl. [CTAB] = 0.008 M, 0.02 mL of seed and $[HAuCl_4] = 1.25 \times 10^{-4}$ M were kept constant in all experiments.

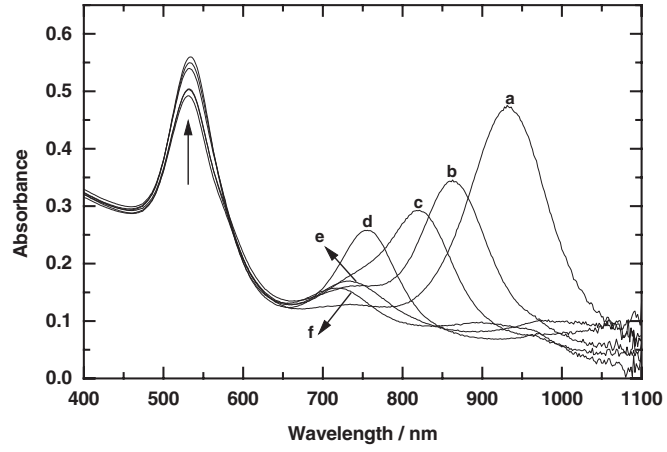


**Figure 7.** Influence of the DTAB concentration on the aspect ratio and yield of the Au nanorods. [CTAB] = 0.008 M, 0.02 mL of seed, and $[HAuCl_4] = 1.25 \times 10^{-4}$ M were kept constant in all experiments; a) 0, b) 1 mM, c) 2 mM, d) 4 mM, e) 8 mM, f) 10 mM DTAB.

added, and therefore the CTAB monomer concentration also increases.

In Figure 8, we present statistical measurements on the rate of growth of both the spheres and the minor and major axes of the rods growing from the seeds. The Figure shows that as more growth solution is added to a seed solution and the aspect

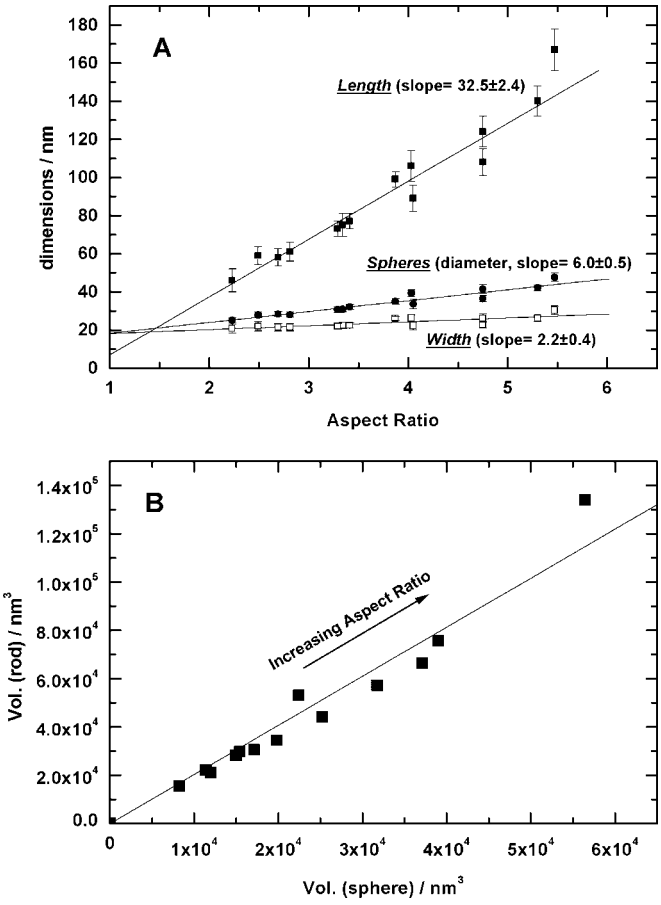


**Figure 8.** A) Dimensions of the rods (length and width) and coexisting spheres for each aspect ratio as determined by TEM for the different seed as listed in Tables S1 and S2 (see Supporting Information). B) Plot of the volume of the rods for each aspect ratio versus the volume of the coexisting spheres. The lines shown are least squares fits to the data.

ratio increases, the rod length grows much faster than the sphere radius, which in turn grows faster than the minor axis of the rods. The volume of the rods, estimated using $V \sim \pi r^2 l$ ($r$: radius, $l$: length) consistently higher than the sphere volume, though both grow from the same seeds by competition for gold salts. This shows that the flux of gold ions to the rods remains higher at all times during growth. This provides the key result that rods form and grow because growth of curved surfaces in the CTAB solution is faster than for flat surfaces.

### 2.6. Binding of Au to CTAB Micelles

A key issue is the binding of the gold ions to the cationic micelles. As shown by other groups, $Au^{III}$–CTAB precipitates at ratios around 1:1, but the $Au^{III}$–CTAB complex is resolubi-

  

lized above the cmc (0.8 mM). Complete solubilization occurs at ratios of about 1:60, which coincides approximately with the micelle aggregation number. Hence the Au–CTAB complex is dissolved when there is one Au–CTAB molecule solubilized in each CTAB micelle. Spectroscopically, the Au complex does not change during resolubilization, so it remains as a tightly bound solute. Esumi and Torigoe found that the solubility constant for $Au^{III}$–CTAB 1:1 complexes is $K \sim 10^{-12}$ M.[25] Typically $<<1$ % of the gold salt is dissolved in solution during rod growth. The $Au^{I}$–CTAB complex, obtained by addition of ascorbic acid to a $Au^{III}$–CTAB solution in a 1:2 ratio, can be isolated by centrifugation and the addition of sodium borohydride to the clear supernatant does not produce any effect, indicating the absence of free $Au^{I}$ in solution. This extremely strong binding of $Au^{I}$ to CTAB is critical for gold rod formation.

Overall, we had little trouble reproducing the main trends of the gold rod synthesis reported by Murphy and coworkers. In addition, we believe the following conclusions can be drawn from the experiments reported here.[26]

1) With colloidally stabilized seeds pre-coated with CTAB, gold nanorods may be reproducibly prepared from the same seed solution for over one month.
2) Decomposition of the excess $NaBH_4$ in the seed solution reduces secondary nucleation during rod growth.
3) The yield of rods improves with increasing colloid stability of the seeds; hence dimers or coalescence are not precursors to rod formation.
4) With stable seeds, homogeneous growth in a stirred, convective solution produces high yields of rods.
5) Bromide alone does not yield rods, but $Br^-$ is much better than $Cl^-$ as a rod-inducing reagent in the presence of $CTA^+$ ions.
6) CTAB is much better than CTAC, $Cl^-$, and DTAB as a rod-inducing surfactant. Longer single-chain cationic surfactants are less efficient due to their reduced solubility in aqueous solution. This can be offset a little by use of higher temperatures. However, the yield of rods decreases gradually at higher temperatures. Similar results have been recently reported by Murphy and coworkers.[27] The addition of NaCl, $NaNO_3$, or NaBr reduces the aspect ratio of the rods, the effects being similar for each ion. An increase in the ionic strength produces a decrease in the yield of rods.
7) Under optimal conditions, the aspect ratio can be controlled directly through seed to $HAuCl_4$ ratios, since there is little nucleation of new particles.
8) The optimal CTAB:$HAuCl_4$ concentration is in a narrow window due to precipitation of CTAB–$HAuCl_4$ at $<10$:1 ratios, while high CTAB concentrations lead to a decrease in aspect ratio due to the increasing bromide ion concentration (point 6).
9) $AgNO_3$ is not needed to control aspect ratio. However, the $AgNO_3$ does increase the yield of rods for the CTAB stabilized seeds, as already pointed out by El-Sayed and coworkers.[14]
10) Both $AuCl_4^-$ and $AuCl_2^-$ are quantitatively adsorbed to CTAB; Esumi and Torigoe have already demonstrated that $AuCl_4^-$ is bound to CTAB.[28]
11) The rate of Au rod formation is orders of magnitude slower than the mass transfer limit, and significantly, it is also orders of magnitude slower than the rate observed for the same system when the seeds grow as spheres in the absence of CTAB.[16] Hence the CTAB not only directs Au to the particle tips, but also drastically retards the rate of metallic gold formation.
12) The higher the curvature of the gold surface, the faster the rate of growth.

## 3. Discussion

### 3.1. The Rate-Determining Step

$AuCl_4^-$ can be reduced to zero valent metal via two distinct pathways. Following reduction of $AuCl_4^-$ to $AuCl_2^-$ via reaction 1, $AuCl_2^-$ may spontaneously disproportionate on the Au colloid surface (reaction 2) or it may be discharged directly through electron transfer at the surface of the electron-rich gold seeds (reaction 3):

$$AuCl_4^- + 2e^- \rightleftarrows AuCl_2^- + 2Cl^- \quad (1)$$

$$3AuCl_2^- \rightleftarrows AuCl_4^- + 2Au^0 + 2Cl^- \qquad K = 15.5 \times 10^7 \quad (2)$$

$$AuCl_2^- + e^- \rightleftarrows 2Au^0 + 2Cl^- \quad (3)$$

We believe the experimental evidence points to reaction 3 as the discharge step. In the presence of CTAB, ascorbic acid reduces $HAuCl_4$ to $AuCl_2^-$, as evidenced by the loss of the 395 nm charge-transfer-to-solvent (CTTS) band and the appearance of a new band at 260 nm; however, no colloidal gold is formed. The solution of $AuCl_2^-$–CTAB remains stable indefinitely, i.e., in a CTAB solution disproportionation of $AuCl_2^-$–CTAB does not occur. In fact, we have found that we can make solutions of $AuCl_2^-$–CTAB by adding $HAuCl_4$ to colloidal gold in the presence of CTAB. In other words, gold colloids are oxidized by $Au^{III}$, and conproportionation occurs rather than disproportionation in the presence of CTAB.[29] The binding constant of $AuCl_2^-$ to CTAB must therefore be extraordinarily high. From the fact that a solution of 0.4 mM $HAuCl_4$ and 0.5 mM Au colloid is completely oxidized in the presence of CTAB, the disproportionation reaction has an equilibrium constant $< 10^{-2}$ M. Hence, we conclude that the disproportionation of $AuCl_2^-$ is not the mechanism for gold deposition or rod growth in CTAB solution.[30] Consequently, the reduction of $Au^{I}$ in the presence of CTAB can be described by the reaction:

$$AuCl_2^-\text{–}CTAB_{mic} + Au_m^- \rightleftarrows Au_{m+1}\text{–}CTAB_{mic} + CTAB_{mic} + 2Cl^- \quad (4)$$

A minimalist approach to the question of rod formation is to ask how reduction proceeds if the ions are bound to micelles in solution? During normal "microelectrode-type deposition", electrons are transferred to the Au particle while dissolved or adsorbed $AuCl_2^-$ ions may pick up an electron at any favorable adsorption site. One usually obtains spherical growth under these circumstances. In the case of CTAB-containing solutions,

  

ADVANCED FUNCTIONAL MATERIALS



the gold seeds or rods are encapsulated in CTAB and the gold ions are likewise micellized in CTAB. The zeta potential of CTAB micelles and CTAB-coated gold surfaces are both around +90 mV.[31] We assume that the rate of rod formation is determined by the frequency of collisions of $AuCl_2^-$-laden cationic micelles with the cationic gold seed particles. This in turn is controlled by the electrical double-layer interaction between the micelles and gold rods. The essential elements are illustrated in Scheme 1. $AuCl_4^-$ ions are reduced on the micelle surface to $AuCl_2^-$ ions, but remain tightly bound. During encounters of micelles with the CTAB-coated Au seed particles, gold ions

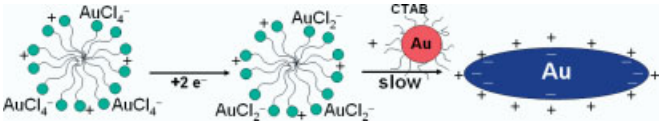


**Scheme 1.** Mechanism for gold rod formation. $AuCl_4^-$ ions are bound to cationic CTAB micelles, displacing $Br^-$ ions. Reduction of $AuCl_4^-$ to $AuCl_2^-$ by ascorbate takes place on the micelle surface. $AuCl_2^-$ remains adsorbed to the micelle. The transport of the bound gold ions to the growing seed particles is controlled by the double layer interaction of the cationic micelles with the micelle-coated gold seeds. This favors deposition at the tips of the seeds, leading to rod formation.

may be discharged. We assume that electron transfer itself is not rate-determining. The rate of reaction is controlled by the collisions of the micelles. If we can show that the rate of collision of the micelles is faster at the tips than the sides, this would provide a direct pathway to rod formation.

### 3.2. Model Calculations

The mean first passage time for a randomly diffusing cationic micelle in the presence of the ellipsoidal gold seed is difficult to calculate. Unlike a single ion, the micelle will modify the distribution of ions within the diffuse layer as it approaches. This will alter the electric field distribution, which in turn will perturb the micelle motion. We content ourselves here with initial calculations of the potential distribution and potential gradient around an ellipsoid in a 1:1, dilute electrolyte. A fuller study of the mass transfer problem is deferred to another paper.

The potential around an ellipsoidal particle can be calculated, for small surface potentials, by solving the Linearized Poisson–Boltzmann (LPB) or Debye–Hückel equation

$$\nabla^2\varphi^2 = \kappa^2\varphi \tag{5}$$

for the scaled potential

$$\varphi = e\psi/kT \tag{6}$$

As usual, $\kappa$ is the inverse Debye length defined by

$$\kappa = (z^2e^2c_o/\varepsilon_r\varepsilon_o kT)^{1/2} \tag{7}$$

where $z$ is the electrolyte valence, $e$ the electronic charge, $c_o$ the electrolyte concentration, $\varepsilon_r$ is the relative dielectric constant of the medium, $\varepsilon_o$ the vacuum permittivity, $k$ Boltzmann's constant and $T$ is the temperature. For metal particles, or surfactant-capped metal particles, we may assume an equipotential surface, i.e., the surface potential will be the same everywhere. We can calculate the potential outside the ellipsoid by placing a continuous distribution of charge along the axis of the ellipsoid interior to the surface (actually between the foci of the ellipsoid).[32] This distribution is chosen to make the surface of the ellipsoid an equipotential surface.

In Figure 9 we show a single quadrant of an ellipsoid and the associated potential distribution for 1 mM salt. The rod is normalized to have a length of one along the major axis. As can be seen the potential decays more rapidly near the tip. Hence it

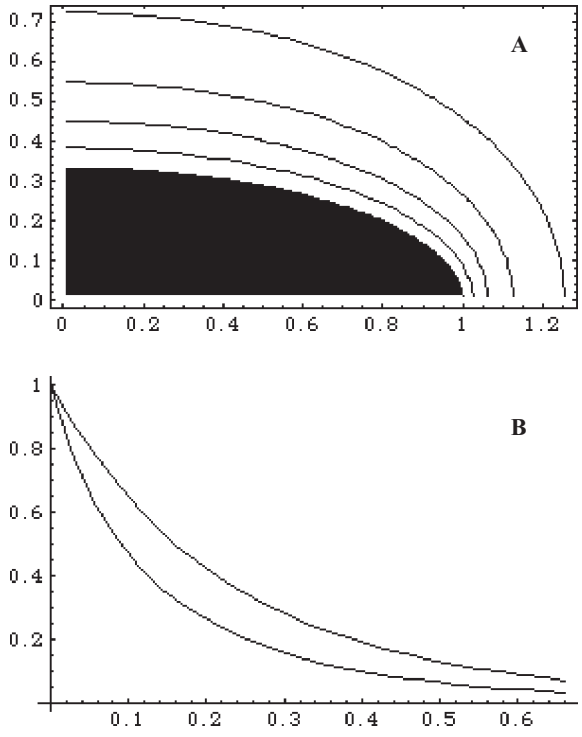


**Figure 9.** A) Contour plot of the potential around a prolate ellipsoid of revolution of aspect ratio 3:1. The scaled surface potential is set to 1 (surface potential is 25 mV) and the contour lines are for $\phi = 0.8, 0.6, 0.4, 0.2$. Position is scaled by the particle semi-major axis $a$ and $\kappa a = 3$. B) Potential profiles $\varphi(x)$ for approach from the side (upper curve) and from the end (lower curve) towards a prolate ellipsoid of revolution of aspect ratio 3:1.

will always be easier for a micelle to approach to a given distance at the tip rather than from the sides of the rods. This is shown more clearly in Figure 9b, which gives the potential profiles $\varphi(x)$ as the ellipsoid is approached from the tip or from the side. Figure 10a shows the same case for an aspect ratio 5 ellipsoid. The potential drop-off is even stronger.

The effect on mass transfer rates of different potential profiles as the ellipsoid is approached from different directions can be quantified approximately by calculating the mean absorption time (MAT) for a point co-ion diffusing in a one-dimensional potential profile $\varphi(x)$ as given in Figure 9b. We consider a co-ion (representing the micelle) to absorb once it

  

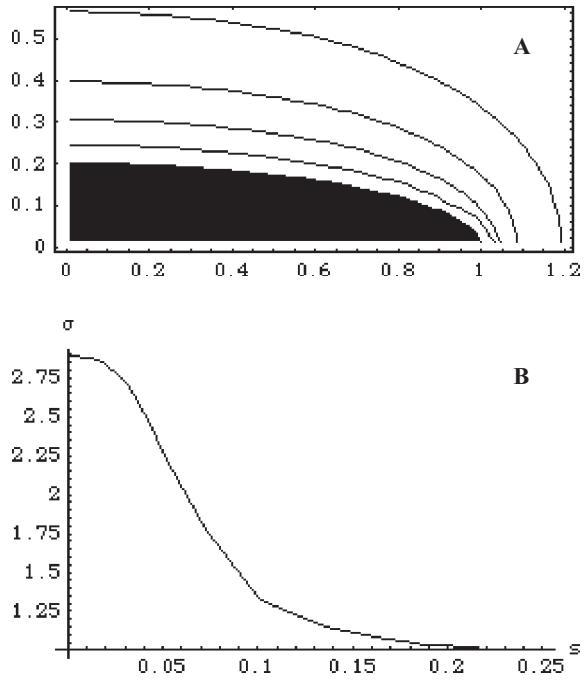


**Figure 10.** A) Contour plot of the scaled potential around a prolate ellipsoid of revolution of aspect ratio 5:1. The scaled surface potential is set to 1 (surface potential is 25 mV) and the contour lines are for $\phi = 0.8$, 0.6, 0.4, 0.2. B) (Scaled) Surface charge density $\sigma$ as a function of angle $2s$, as $s$ goes from 0 (the tip) to 1/4 (the side). $\sigma$ has been scaled by the value at the side, showing the tip enhancement.

reaches the particle surface ($x = 0$) and to be reflected once it reaches some distance $x = b$ at which diffusion is essentially free. Then the MAT, $\tau$, can be expressed in terms of various integrals of the potential profiles[33]

$$\tau = \int_0^b \mathrm{d}x\, e^{\varphi(x)} \left[ \int_x^b \mathrm{d}x'\, e^{-\varphi(x')} \right]^2 \Bigg/ \int_0^b \mathrm{d}x''\, e^{-\varphi(x'')} \tag{8}$$

Here we take $b$ to be a position where the potential is small compared to $kT$, for example

$$\varphi(b) = 0.05kT \tag{9}$$

Then, $b$ is significantly smaller for approach to the tip, leading to smaller MATs and hence faster growth rates if mass transfer is rate-limiting. Evaluating $\tau$ using surface potentials in the range 25–50 mV and criteria for $b$ in the range 0.05–0.1 $kT$, we get faster rates at the tips by factors of 1.85–2.1 for 3:1 ellipsoids and 2.2–2.9 for 5:1 ellipsoids.

Since the field at the tip is stronger, this might seem a strange result. The co-ions are all diffusing up an energy barrier, against the field. Since the surface is equipotential, the barrier height is the same for all directions of approach. Because the potential falls off faster at the tip, the co-ion is closer to the surface before it has begun to climb the barrier, leaving a shorter distance to cover by random fluctuations to reach the surface. This is why the MAT is smaller if approach is towards the tip than towards the side.

Such a one-dimensional treatment can only be suggestive of what happens in the general case, which would require much more detailed computations. Note this factor-of-three difference is for a single test charge. The cationic micelle will have a charge of perhaps +60. The surface potential is +90 mV. The enhancement is then expected to be orders of magnitude higher, but the LPB and MAT calculations here will break down under such extreme conditions.

The other factor of interest is the surface charge density on the particle. The surface charge density is directly related to the local electric field by

$$\sigma_o = -\varepsilon_r \varepsilon_o \left. \frac{\mathrm{d}\psi}{\mathrm{d}x} \right|_{x=0} \tag{10}$$

In Figure 10b, we plot the surface charge density near the surface as a function of the angle $2s$ around the particle, starting from the tip ($s = 0$) and falling to the value at the side ($s = 1/4$). The values have been scaled by the value at the side, to show the field enhancement at the tip. For the low potentials considered here, the surface charge density and hence the field strength scale linearly with aspect ratio. This is the mechanism, which provides for continuous rod growth and large aspect ratios. Rod formation automatically ensues as a consequence of the double-layer interaction between the micelles and the particles. Though the electric potential of the gold seed will be constant, the changing curvature requires that the electric field will be higher on points of high curvature. As soon as nanorod formation begins, it will self-catalyze elongation, since preferential reduction at any site will increase the curvature at that point, so that deposition is even faster. Electric-field-directed growth then leads to rod formation.

### 3.3. Symmetry Breaking

The importance of the double layer in rod formation helps to resolve the effects of salt on the rod formation. Anything, which diminishes the free energy of the micelle–gold interaction, will weaken the selectivity for rods. Higher temperature, added salts, or salts that solubilize the $Au^{III}$ will lead to spherical particles. Longer-chain analogues of CTAB should be useful for rod formation, but their solubility in aqueous solutions is so low that they are impractical. Shorter-chain analogues, such as DTAB, have higher cmcs, and consequently gold ions are more soluble in these solutions leading to poorer selectivity for rod formation. We note that the frequency of collisions between large cationic micelles and the positively charged gold particles will be orders of magnitude lower than for free $AuCl_2^-$ ions diffusing to a seed particle, and this readily explains the sluggish kinetics of rod growth (Fig. 2).

The model does not explain explicitly the initial change in morphology. A charged sphere will have a symmetric electric field distribution and hence spherical growth should prevail. However, the real seed is typically a cuboctahedron with [100] and [111] faces predominant and with well-defined edges between them and charge discontinuities. It may be that a stacking fault or twinning plane in the seed is also necessary to create an initial electric field asymmetry.

  

## 4. Conclusion

In summary, we have shown that $Au^{III}$ is bound to CTAB micelles. On addition of ascorbate, $Au^{III}$ is reduced to $Au^{I}$, which in turn is bound even more strongly to CTAB micelles, and this has been confirmed by the finding that all $Au^{I}$ can be centrifuged out of the solution when CTAB is present. These micelles have an extremely low collision frequency with the gold seeds, which causes the rate of growth to be retarded by several orders of magnitude. In turn the slow collision frequency and the enhanced electric field at the tip allows reduction of $Au^{I}$ to take place almost exclusively at the termini. Maximum selectivity occurs at low temperatures and low ionic strength.

We have optimized the preparation of gold nanorods by exploring the parameters that induce spherical seeds to become gold rods. There is no evidence for a direct surfactant templating mechanism, such as may occur in inverse micelles, since gold rod formation occurs well below the CTAB concentration at which the sphere-to-rod transition occurs. The idea that CTAB simply lowers the interfacial tension of a particular crystal facet is difficult to exclude but the sensitivity of the rod formation to temperature and $Cl^-$ concentration suggest that the quantitative binding of $Au^{III}$ and $Au^{I}$ to the cationic micelles is the dominant effect.

## 5. Experimental

*Chemicals*: Ascorbic acid, cetyltrimethylammonium bromide (CTAB), and $NaBH_4$ were supplied from Aldrich. $HAuCl_4 \cdot 3H_2O$ and trisodium citrate dihydrate were supplied from Sigma. Sodium chloride was supplied from Fluka. Cetyltrimethylammonium chloride (CTAC) and dodecyltrimethylammonium bromide (DTAB) were supplied from Kodak Specialty Chemicals. All reactants were used without further purification. Milli-Q water was used in all the preparations.

*Preparation of 3.5 nm Au Citrate Seed Particles*: A 20 mL aqueous solution containing $1.25 \times 10^{-4}$ M $HAuCl_4$ and $2.50 \times 10^{-4}$ M trisodium citrate was prepared in a conical flask at room temperature. Next, 0.3 mL of ice-cold, freshly prepared 0.01 M $NaBH_4$ solution was added to the solution while vigorous stirring. The stirring was slowed down after 30 s and for the next 15 min the Au sol was stirred gently at 40–45 °C to ensure removal of excess $NaBH_4$. The 3.5 nm seed solution can be used for up to a month.

*Preparation of 5.5 nm Au–CTAB Seed Particles*: 5 mL of growth solution consisting of $1.25 \times 10^{-4}$ M $HAuCl_4$ and 0.040 M CTAB thermostatted at 25–30 °C was mixed under stirring with 0.0125 mL of 0.10 M ascorbic acid. 1.67 mL of 3.5 nm Au citrate seed solution was then added quickly to the solution while stirring.

*Preparation of 7.0 nm Au–CTAB Seed Particles*: 5 mL of growth solution consisting of $1.25 \times 10^{-4}$ M $HAuCl_4$ and 0.040 M CTAB thermostatted at 25–30 °C was mixed under stirring with 0.0125 mL of 0.10 M ascorbic acid. 0.625 mL of 3.5 nm Au citrate seed solution was then added quickly to the solution while stirring. In the Supporting Information we present the spectra of these seeds (Figure S1). The broader blue-shifted plasmon band is expected for small gold particles.

*Growth of Gold Nanorods*: (see Fig. 1) The different solutions (a–h) were prepared using 10 mL of growth solution ($[HAuCl_4] = 1.25 \times 10^{-4}$ M and $[CTAB] = 0.008$ M), thermostatted at 20 °C. Next 0.025 mL of 0.1 M ascorbic acid was added to each solution and mixed thoroughly. Finally different volumes of 3.5 nm Au citrate seed solution were added (0.010, 0.015, 0.020, 0.030, 0.040, 0.060, 0.080, and 0.10 mL).

*Instrumentation*: Absorption spectra of the solutions were measured using a CARY 50 Scan UV-vis-NIR or a HP8453 UV-vis spectrophotometer. Transmission electron microscopy (TEM) images were acquired with a Philips CM 10 microscope, and particles size distribution was measured from several TEM negatives from each sample (1500–2000 spheres and 1500–2000 rods where measured for each sample). Sizing was carried out using a Nikon digital camera with Matrix 3.0v software. For TEM preparation, the excess surfactant present in the particle solution was removed by centrifuging 2 mL of the particle solution at 9000 rpm for 10 min. The supernatant containing surfactant was discarded and the precipitate redispersed in 2 mL of water. It was again centrifuged at 2800 rpm for 10 min and redispersed in 0.25 mL of water. Next, a drop of the particle solution was placed on a formvar-coated copper grid and dried at room temperature.

Received: October 1, 2003
Final version: April 19, 2004

[1] G. Frens, *Nature Phys. Sci.* **1973**, *241*, 20.
[2] G. S. Metraux, Y. C. Cao, R. Jin, C. A. Mirkin, *Nano Lett.* **2003**, *3*, 519.
[3] I. Pastoriza-Santos, L. M. Liz-Marzan, *Nano Lett.* **2002**, *2*, 903.
[4] A. Filankembo, M. P. Pileni. *J. Phys. Chem. B* **2000**, *104*, 5865.
[5] C. Schoenenberger, B. M. I. van der Zande, L. G. J. Fokkink, M. Henny, C. Schmid, M. Krueger, A. Bachtold, R. Huber, H. Birk, U. Staufer, *J. Phys. Chem. B* **1997**, *101*, 5497.
[6] V. M. Cepak, C. R. Martin, *J. Phys. Chem. B* **1998**, *102*, 9985.
[7] N. Al-Rawashdeh, C. A. Foss Jr., *Nanostruct. Mater.* **1997**, *9*, 383.
[8] Y.-Y. Yu, S.-S. Chang, C.-L. Lee, C. R. C. Wang, *J. Phys. Chem. B* **1997**, *101*, 6661.
[9] S.-S. Chang, C.-W. Shih, C.-D. Chen, W.-C. Lai, C. R. C. Wang, *Langmuir* **1999**, *15*, 701.
[10] N. R. Jana, L. Gearheart, C. J. Murphy, *Chem. Commun.* **2001**, 617.
[11] N. R. Jana, L. Gearheart, C. J. Murphy, *Adv. Mater.* **2001**, *13*, 1389.
[12] F. Kim, J. H. Song, P. Yang, *J. Am. Chem. Soc.* **2002**, *124*, 14 316.
[13] Murphy and colleagues have subsequently reported preparation conditions in which silver was not required, though heptane was employed to create longer aspect ratios (e.g., B. D. Busbee, S. O. Obare, C. J. Murphy, *Adv. Mater* **2003**, *15*, 414.)
[14] B. Nikoobakht, M. A. El-Sayed, *Chem. Mater.* **2003**, *15*, 1957.
[15] S. Biggs, P. Mulvaney, C. F. Zukoski, F. Grieser, *J. Am. Chem. Soc.* **1994**, *116*, 9150.
[16] N. R. Jana, L. Gearheart, C. J. Murphy, *Chem. Mater.* **2001**, *13*, 2313.
[17] N. R. Jana, L. Gearheart, C. J. Murphy, *J. Phys. Chem. B* **2001**, *105*, 4065.
[18] K. Torigoe, K. Esumi, *J. Phys. Chem. B* **1999**, *103*, 2862.
[19] D. G. Duff, A. Baiker, P. P. Edwards, *Langmuir* **1993**, *9*, 2301.
[20] N. R. Jana, L. Gearheart, C. J. Murphy, *Langmuir* **2001**, *17*, 6782.
[21] J. D. Morgan, D. H. Napper, G. G. Warr, S. K. Nicol, *Langmuir* **1994**, *10*, 797.
[22] F. M. Menger, D. Y. Williams, A. L. Underwood, E. W. Anacker, *J. Colloid Interface Sci.* **1982**, *90*, 546.
[23] F. Quirion, L. J. Magid, *J. Phys. Chem.* **1986**, *90*, 5435.
[24] H. N. Patrick, G. G. Warr, S. Manne, I. A. Aksay, *Langmuir* **1999**, *15*, 1685.
[25] K. Esumi, K. Matsuhisa, K. Torigoe, *Langmuir* **1995**, *11*, 3285.
[26] For simplicity, we will assume that $Au^{III}$ is in the $AuCl_4^-$ form, although some hydrolysis definitely occurs, (C. F. Baes, R. E. Mesmer, in *The Hydrolysis of Cations*, Robert E. Krieger Publishing Co., Malabar, FL **1986**, p. 284) and likewise we will treat $Au^{I}$ as though it is exclusively in solution as $AuCl_2^-$.
[27] J. Gao, C. M. Bender, C. J. Murphy, *Langmuir* **2003**, *19*, 9065.
[28] K. Esumi, K. Torigoe, *Langmuir* **1992**, *8*, 59.
[29] C. H. Gammons, Y. M. Yu, A. E. Wiliams Jones, *Geochim. Cosmochim. Acta* **1997**, *61*, 1971.
[30] However disproportionation may be the active mechanism for colloidal gold formation in the absence of CTAB.
[31] S. Biggs, P. Mulvaney, *J. Chem. Phys.* **1994**, *100*, 8501.
[32] M. Teubner, J. Frahm, *J. Colloid Interface Sci.* **1981**, *82*, 560.
[33] D. Y. C. Chan, B. Halle, *Biophys. J.* **1984**, *42,* 387.

  